Title

Structural and spectroscopic characterization of an einsteinium complex

Journal

Nature, 590(7844)

ISSN

0028-0836

Authors

Carter, Korey P

Shield, Katherine M

Smith, Kurt F

et al.

Publication Date

2021-02-04

DOI

10.1038/s41586-020-03179-3

Peer reviewed

Structural and spectroscopic characterization of an einsteinium complex

https://doi.org/10.1038/s41586-020-03179-3

Received: 3 July 2020

Accepted: 29 October 2020

Check for updates

Korey P. Carter[1], Katherine M. Shield[1,2], Kurt F. Smith[1], Zachary R. Jones[3], Jennifer N. Wacker[3,4], Leticia Arnedo-Sanchez[1], Tracy M. Mattox[5], Liane M. Moreau[1], Karah E. Knope[4], Stosh A. Kozimor[3]✉, Corwin H. Booth[1]✉ & Rebecca J. Abergel[1,2]✉

The transplutonium elements (atomic numbers 95–103) are a group of metals that lie at the edge of the periodic table. As a result, the patterns and trends used to predict and control the physics and chemistry for transition metals, main-group elements and lanthanides are less applicable to transplutonium elements. Furthermore, understanding the properties of these heavy elements has been restricted by their scarcity and high radioactivity. This is especially true for einsteinium (Es), the heaviest element on the periodic table that can currently be generated in quantities sufficient to enable classical macroscale studies[1]. Here we characterize a coordination complex of einsteinium, using less than 200 nanograms of ^{254}Es (half-life of 275.7 days), with an organic hydroxypyridinone-based chelating ligand. Structural studies are used to determine the energy of the L_3 absorption edge and a bond distance of einsteinium. Photophysical measurements reveal antenna sensitization of Es^{III} luminescence; they also reveal a hypsochromic shift on metal complexation, which had not previously been observed in lower-atomic-number actinide elements. These findings are indicative of an intermediate spin–orbit coupling scheme in which *j*–*j* coupling (whereby single-electron orbital angular momentum and spin are first coupled to form a total angular momentum, *j*) prevails over Russell–Saunders coupling. Together with previous actinide complexation studies[2], our results highlight the need to continue studying the unusual behaviour of the actinide elements, especially those that are scarce and short-lived.

The high radioactivity and scarcity of Es isotopes have precluded this element from receiving the same attention as its preceding neighbours within the actinide series, the bonding, electronic structure and chemical properties of which are assumed to be between those of the transition metals and the lanthanides[1]. This unusual chemical behaviour is often attributed to the emergence of the 5*f* orbital manifold, large spin–orbit coupling and substantial relativistic effects[3], and all these properties are known to increase across the actinide series[4]. Contemporary worldwide availability of Es is restricted to small-scale quantities (nano- to micrograms) of one of its two long-lived isotopes, ^{254}Es (half-life $t_{1/2}$ = 275.7 days), the decay rate of which is roughly 300 times faster than that of its longer-lived transplutonium neighbour, ^{249}Cf (ref. [5]). However, there are some examples that demonstrate how the technical challenges associated with working with transplutonium elements can be overcome, even for less accessible elements such as Es. Highlights from the few previous Es studies include establishing nuclear properties from Es isotopes[6], purifying Es from neighbouring actinides[7–9], and initial reporting of various ionization potentials and thermodynamic properties of Es[1,10]. A few simple inorganic compounds—oxides and halides—of Es have been prepared. These compounds were characterized in terms of their unit-cell parameters; some optical measurements have also been reported[1,11–14]. Furthermore, thermodynamic stability constants have been measured for a limited series of common complexing agents (Cl^-, OH^-, SO_4^{2-} and SCN^-) and chelators (ethylenediaminetetraacetic acid and diethylenetriaminepentaacetic acid), using radioactive tracer methods[1,15–18]. Beyond this, the chemistry of Es is unexplored and so there is insufficient experimental data to validate theoretical predictions regarding structure and bonding. One reason it is difficult to make accurate predictions for Es is because of its location in the actinide series. For example, it is unclear which oxidation states will be stable in numerous chemical environments because Es lies between larger minor actinides (Am, Cm, Bk and Cf) that favour the +3 oxidation state and smaller late actinides (Fm, Md, No and Lr), for which the +2 oxidation state becomes increasingly accessible[3]. Predicting changes in reactivity and electronic structureduring a chemical process is rarely possible for Es because—in comparison to other actinides—its Lewis acidity is large, its ionic radius is small and it has a substantial number of unpaired 5*f* electrons (Es^{III} is (Rn) $5f^{10})^2$.

Here we report how we overcame the challenges of working with small quantities of ^{254}Es (less than 200 ng) to enable the characterization of an Es coordination complex in solution and as a solid. We chose the octadentate hydroxypyridinone ligand 3,4,3-LI(1,2-HOPO) (HOPO;

[1]Chemical Sciences Division, Lawrence Berkeley National Laboratory, Berkeley, CA, USA. [2]Department of Nuclear Engineering, University of California, Berkeley, CA, USA. [3]Los Alamos National Laboratory, Los Alamos, NM, USA. [4]Department of Chemistry, Georgetown University, Washington, DC, USA. [5]Molecular Foundry, Lawrence Berkeley National Laboratory, Berkeley, CA, USA. ✉e-mail: stosh@lanl.gov; chbooth@lbl.gov; abergel@berkeley.edu

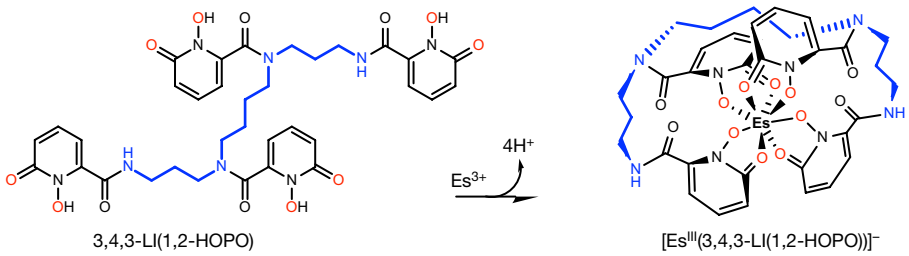

Fig. 1 | The organic ligand 3,4,3-LI(1,2-HOPO) forms an Es^{III} coordination complex, enabling structural and spectroscopic studies. The octadentate chelator is composed of four 1-hydroxy-pyridin-2-one metal binding units attached to a spermine scaffold (blue) through amide linkages. Eight metal-binding O atoms (red) serve as the first coordination sphere around Es^{III} on ligand deprotonation and metal complexation.

Fig. 1) as the complexing agent, because of its well established chelation properties with transition metals and *f* elements, and its propensity to act as a luminescence sensitization antenna. The latter characteristic enabled the detection of the luminescence spectrum of Es, even with less than 100 ng available for study. Luminescence measurements strongly suggest that Es was in the +3 oxidation state when chelated by HOPO. These optical results complement structural characterization of the corresponding complex using trace-level X-ray absorption spectroscopy (XAS) measurements at the Stanford Synchrotron Radiation Lightsource.

For XAS studies, ^{254}Es (17 µM, 40 µl) was complexed with HOPO at a 1:10 metal-to-ligand ratio in aqueous solution buffered at pH 7–8 to ensure full ligand deprotonation and the formation of a single Es species, $[Es^{III}(HOPO)]^-$ (Fig. 1). The solution was then dropcast into a 3D-printed sample holder. The resulting solid residue was triply contained and the sample was cooled with liquid nitrogen (about 77 K), before the L_3-edge XAS spectrum of Es was collected in fluorescence mode. Balancing moderate brightness from the Stanford Synchrotron Radiation Lightsource with the trace-level detection capabilities of the

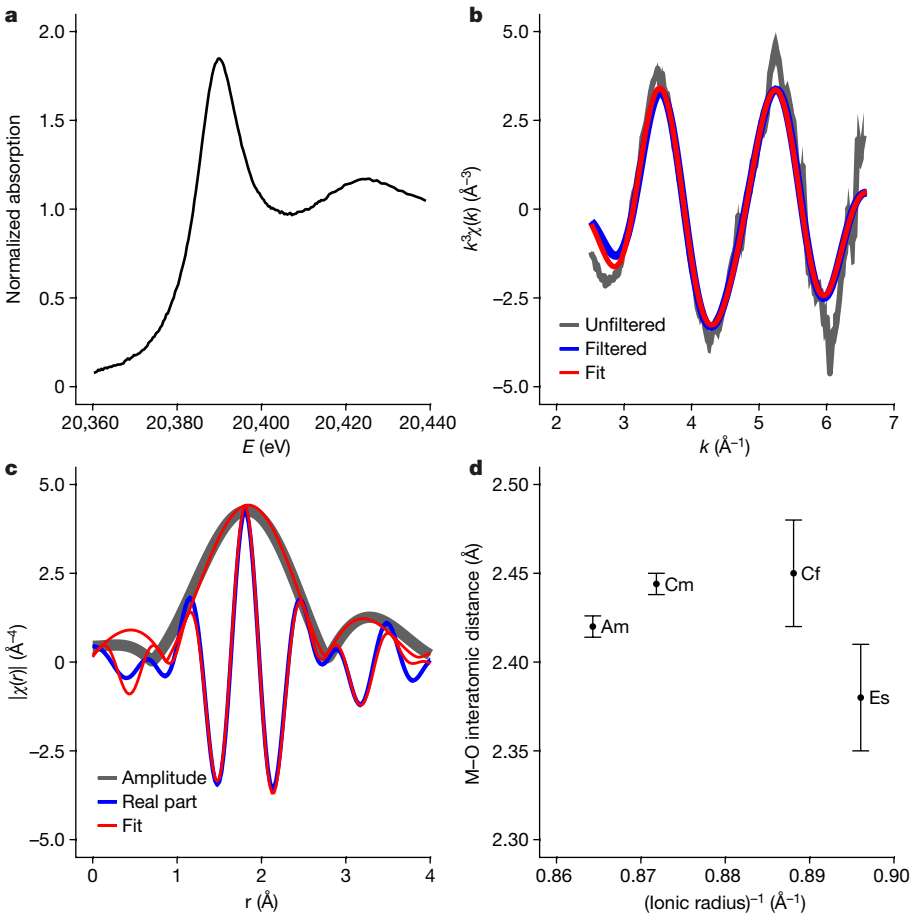

Fig. 2 | The structural features of the $[Es^{III}(HOPO)]^-$ coordination complex were probed using element-specific L_3-edge XAS at 77 K. a–**c**, XANES spectrum (**a**), EXAFS data and fit (**b**), and Fourier transform of the *k*-space data and fit (**c**) for solid residue of $[Es^{III}(HOPO)]^-$. *E* is the incident photon energy, $k^3\chi(k)$ is the EXAFS function and *r* represents the scattering distance (not phase-corrected). Fits were obtained as described in Methods. Data were transformed between 2.5 $Å^{-1}$ and 6.6 $Å^{-1}$ using a Gaussian window with a width of 0.3 $Å^{-1}$. Error bars for the raw, unfiltered data are estimated as the standard deviation of the mean between individual traces. The full data range for the raw data is shown in Extended Data Fig. 2. **d**, The Es–O bond distance was validated against bond lengths determined from previously characterized $[M^{III}(HOPO)]^-$ (M = Am, Cm, Cf) complexes, with a coordination number of 9, highlighting a substantially shorter M–O bond in the Es complex[2]. Ionic radii taken from ref. [26]. Error bars are based on a profiling method[28] from the fit, together with an estimate of probable systematic error from the limited *k* range.

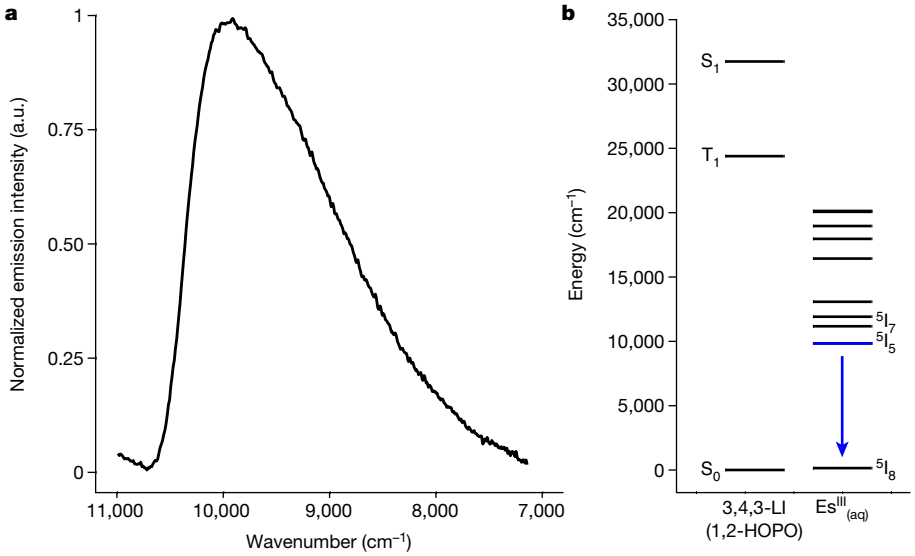

Fig. 3 | Luminescence sensitization of Es was achieved on chelation by HOPO, confirming the +3 oxidation state for Es and revealing an unusual hypsochromic shift in metal emission. a, Normalized emission of $[Es^{III}(HOPO)]^-$ in 1 M TRIS, pH 7–8, at 298 K, on excitation at a wavelength of $\lambda = 320$ nm with a Y48 bandpass filter ($\lambda = 480 \pm 5$ nm). a.u., arbitrary units. **b**, Energy-level diagram for complexed HOPO and $Es^{III}_{(aq)}$ (refs. [21,27]). The blue arrow depicts the transition from the first excited electronic energy level to the ground state.

100-element Ge detector on beamline 11-2 enabled data collection over 84 h at the L_3 edge of Es, using only 175 ng of ^{254}Es. The X-ray absorption near-edge structure (XANES) spectrum from $[Es^{III}(HOPO)]^-$ showed no systematic changes with time, which indicates a lack of observable evidence of beam-induced damage. The L_3-edge energy of Es was predicted in 1967 to be 20,410 eV, using Slater–Dirac energy-level calculations[19]; we measured this absorption edge using $[Es^{III}(HOPO)]^-$ (Fig. 2). Energies for the main absorption peak maximum (white line) and the inflection point (E_0, which directly corresponds to the binding energy of the $2p_{3/2}$ core shell of the ionized electrons) were determined to be 20,390.0(1) eV and 20,385.4(2) eV, respectively (calibrated to the K edge of a Mo reference foil, 20,000.0 eV; numbers in parentheses indicate one standard deviation in the distribution determined from many measurements). Both values are broadly consistent with the previous calculations[19]. Because Es samples have not previously been measured, the XANES results cannot be used to establish valence, which is normally determined with XANES by comparing to known standard materials. However, because optical measurements (see below) confirm that the Es in $[Es^{III}(HOPO)]^-$ is Es^{III}, the XANES measurement provides an Es^{III} reference point to evaluate Es oxidation states in other compounds within various matrices. In addition, the shape of the XANES spectrum is very similar to those from other measured $[An^{III}(HOPO)]^-$ complexes (Extended Data Fig. 1).

We characterized the local structure around the metal cation in the $[Es^{III}(HOPO)]^-$ complex using the L_3-edge extended X-ray absorption fine structure (EXAFS) of Es (Fig. 2, Extended Data Table 2). The results are consistent with complexation of Es^{III} by HOPO. The spectrum has two features in the Fourier transform of the data, at around 1.8 Å and 3.2 Å; we developed an appropriate model for these data on the basis of previously calculated $[M^{III}(HOPO)]^-$ complexes[2]. The model includes eight O atoms in the first shell and a combination of four C and four N atoms in the second shell. Because the coordination environment around Es is assumed to be due to HOPO complexation, we expect four C and four N atoms at nearly the same bond length. The spatial resolution of the data is only 0.24 Å, so the shells are fully constrained together. The C and N line shapes are still used for completeness, even though the line shapes for these elements are nearly identical (Methods). Given this model, the fit to the transformed data results in an average Es–O bond distance of 2.38(3) Å (Debye Waller factor $\sigma^2 = 0.009(2)$ Å^2) and an average Es–C or Es–N distance of 3.40(3) Å ($\sigma^2 = 0.012(7)$ Å^2). Owing to the challenges of modelling EXAFS data with such a limited range of photoelectron wavevectors, k, we validated the Es–O bond distance from our model against previously determined M–O bond lengths in $[M^{III}(HOPO)]^-$ (M = Am, Cm, Cf) complexes as a function of the maximum wavevector (k_{max}) used to fit the EXAFS data (Fig. 2)[2]. All three actinide complexes show changes in best-fitting bond distance as a function of k_{max} before stabilizing at about 7 Å^{-1}, with the most extreme variations observed for Am and Cf. In those cases, the stable Am–O and Cf–O distances ($k_{max} > 7$ Å^{-1}) were only around 0.03 Å different from datasets with $k_{max} = 6.5$ Å^{-1} (Extended Data Fig. 3). On the basis of these analyses, we estimate the uncertainty in the Es–O bond distances to be roughly 0.03 Å. The short k_{max} of these data precludes further analysis of σ^2 in the fit (Methods). However, the EXAFS-measured Es–O bond distance is representative of all eight $M–O_{HOPO}$ distances, which vary by up to 0.1 Å for metals with ionic radii similar to that of Es (such as Eu^{III})[20].

Interpretation of the L_3-edge XAS data was guided by complementary solution-phase luminescence spectroscopy on the same $[Es^{III}(HOPO)]^-$ complex. Following optical investigations of Es^{III} doped into GdI_3 crystals[13], it was demonstrated that Es^{III} could be sensitized via the antenna effect in Es-doped $CsGd(hfac)_4$ crystals (hfac = hexafluoroacetylacetonate)[14], which until now was the sole example of Es luminescence sensitization. On excitation of the $[Es^{III}(HOPO)]^-$ sample at 31,250 cm^{-1}, we observed a single, broad peak at 9,950 cm^{-1}. We assign this feature to a transition from the first excited electronic energy level ($J = 5$) to the ground state ($J = 8$) of Es^{III} (Fig. 3), which we attribute to the $^5I_5 \rightarrow {}^5I_8$ transition. This optical response confirms the complexation of Es in the +3 oxidation state by HOPO[21]; although the broadness of the $^5I_5 \rightarrow {}^5I_8$ peak is atypical for $f \rightarrow f$ transitions, it is consistent with the only other example of aqueous Es^{III} luminescence[22] and could be a result of the wide slit widths (Methods) that were necessary to obtain the spectrum highlighted in Fig. 3. In contrast with observations from other +3 f-block cations, the spectral peak of $[Es^{III}(HOPO)]^-$ is not bathochromically shifted when compared to the Es-aquo ion, which has a luminescence maximum of 9,259.3 cm^{-1} (ref. [22]). Instead, HOPO complexation induced a blueshift (+690.7 cm^{-1}) that is consistent with, but almost an order of magnitude larger than, the 77.8 cm^{-1} blueshift reported for Es-doped $CsGd(hfac)_4$ (9,337.1 cm^{-1})[14]. Although these examples of blueshifted Es^{III} luminescence seem to contradict the nephelauxetic effect, the $^5I_5 \rightarrow {}^5I_8$

transition is known to be hypersensitive. Hence, changes in crystal field and spin–orbit coupling could result in hyperfine splitting of the first excited and ground states of Es^{III}, thereby changing the energy gap between these two levels and resulting in a hypsochromic shift[23,24]. Such behaviour is very different from the redshifted luminescence often reported when binding lanthanides and earlier +3 actinides (Am or Cm), for which Russell–Saunders coupling is known to dominate. It is possible that these shifts to higher wavenumbers observed on Es complexation are due to an increase in effective nuclear charge, resulting from an intermediate coupling scheme in which *j*–*j* coupling prevails over Russell–Saunders coupling[25]. Such a transition to a different spin–orbit coupling regime from the $5f^6$ Am^{III} and $5f^7$ Cm^{III} (and $5f^7$ Bk^{IV}) ions to $5f^{10}$ Es^{III} would be remarkable. Near-infrared luminescence spectroscopy experiments with $5f^9$ Cf^{III} and multiconfigurational complete active-space self-consistent field (CASSCF) calculations will be used to explore this behaviour in future studies.

In summary, we have synthesized and characterized an Es coordination complex using complementary X-ray absorption and luminescence spectroscopies. XANES and EXAFS measurements on $[Es^{III}(HOPO)]^-$ provided an experimental measurement of the L_3-absorption-edge energy of Es and of an Es bond distance. Luminescence spectroscopy results revealed another instance of Es sensitization, via the antenna effect, with hypsochromic luminescence shifts evidenced in both systems on metal complexation, which is unprecedented for +3 actinide (and lanthanide) HOPO luminescence. Combined with the short Es–HOPO bond distances and XANES analyses, the sensitive Es^{III} luminescence underlines the potential differences between Es and the rest of the actinides. Finally, because all data were collected with less than 200 ng of metal, our results highlight the potential to advance coordination chemistry across the actinide series and the periodic table when samples are available in only limited quantities.

Online content

Any methods, additional references, Nature Research reporting summaries, source data, extended data, supplementary information, acknowledgements, peer review information; details of author contributions and competing interests; and statements of data and code availability are available at https://doi.org/10.1038/s41586-020-03179-3.

1. Haire, R. G. in *The Chemistry of the Actinide and Transactinide Elements* (eds Morss, L. R. et. al) 1577–1620 (Springer, 2011).
2. Kelley, M. P. et al. Bond covalency and oxidation state of actinide ions complexed with therapeutic chelating agent 3,4,3-LI(1,2-HOPO). *Inorg. Chem.* **57**, 5352–5363 (2018).
3. Hulet, E. K. Chemistry of the elements einsteinium through element-105. *Radiochim. Acta* **32**, 7–24 (1983).
4. Pyykko, P. Relativistic effects in structural chemistry. *Chem. Rev.* **88**, 563–594 (1988).
5. Ferguson, D. E. ORNL transuranium program: the production of transuranium elements. *Nucl. Sci. Eng.* **17**, 435–437 (1963).
6. Meierfrankenfeld, D., Bury, A. & Thoennessen, M. Discovery of scandium, titanium, mercury, and einsteinium isotopes. *At. Data Nucl. Data Tables* **97**, 134–151 (2011).
7. Thompson, S. G., Harvey, B. G., Choppin, G. R. & Seaborg, G. T. Chemical properties of elements 99 and 100. *J. Am. Chem. Soc.* **76**, 6229–6236 (1954).
8. Choppin, G. R., Harvey, B. G. & Thompson, S. G. A new eluant for the separation of the actinide elements. *J. Inorg. Nucl. Chem.* **2**, 66–68 (1956).
9. Horwitz, E. P., Bloomquist, C. A. A. & Henderson, D. J. The extraction chromatography of californium, einsteinium, and fermium with di(2-ethylhexyl)orthophosphoric acid. *J. Inorg. Nucl. Chem.* **31**, 1149–1166 (1969).
10. Peterson, J. R. et al. Determination of the first ionization potential of einsteinium by resonance ionization mass spectroscopy (RIMS). *J. Alloys Compd.* **271–273**, 876–878 (1998).
11. Haire, R. G. & Baybarz, R. D. Identification and analysis of einsteinium sesquioxide by electron diffraction. *J. Inorg. Nucl. Chem.* **35**, 489–496 (1973).
12. Fellows, R. L., Peterson, J. R., Noé, M., Young, J. P. & Haire, R. G. X-ray diffraction and spectroscopic studies of crystalline einsteinium(III) bromide, $^{253}EsBr_3$. *Inorg. Nucl. Chem. Lett.* **11**, 737–742 (1975).
13. Gutmacher, R. G., Evans, J. E. & Hulet, E. K. Sensitive spark lines of einsteinium. *J. Opt. Soc. Am.* **57**, 1389–1390 (1967).
14. Nugent, L. J., Baybarz, R. D., Werner, G. K. & Friedman, H. A. Intramolecular energy transfer and sensitized luminescence in an einsteinium β-diketone chelate and the lower lying electronic energy levels of Es(III). *Chem. Phys. Lett.* **7**, 179–182 (1970).
15. Harmon, H. D., Peterson, J. R. & McDowell, W. J. The stability constants of the monochloro complexes of Bk(III) and Es(III). *Inorg. Nucl. Chem. Lett.* **8**, 57–63 (1972).
16. Harmon, H. D., Peterson, J. R., McDowell, W. J. & Coleman, C. F. The tetrad effect: the thiocyanate complex stability constants of some trivalent actinides. *J. Inorg. Nucl. Chem.* **34**, 1381–1397 (1972).
17. McDowell, W. J. & Coleman, C. F. The sulfate complexes of some trivalent transplutonium actinides and europium. *J. Inorg. Nucl. Chem.* **34**, 2837–2850 (1972).
18. Kelley, M. P. et al. Revisiting complexation thermodynamics of transplutonium elements up to einsteinium. *Chem. Commun.* **54**, 10578–10581 (2018).
19. Bearden, J. A. & Burr, A. F. Reevaluation of X-ray atomic energy levels. *Rev. Mod. Phys.* **39**, 125–142 (1967).
20. Daumann, L. J. et al. New insights into structure and luminescence of Eu^{III} and Sm^{III} complexes of the 3,4,3-LI(1,2-HOPO) ligand. *J. Am. Chem. Soc.* **137**, 2816–2819 (2015).
21. Carnall, W. T., Cohen, D., Fields, P. R., Sjoblom, R. K. & Barnes, R. F. Electronic energy level and intensity correlations in the spectra of the trivalent actinide aquo ions. I. Es^{3+}. *J. Chem. Phys.* **59**, 1785–1789 (1973).
22. Beitz, J. V., Wester, D. W. & Williams, C. W. 5*f* state interaction with inner coordination sphere ligands: Es^{3+} ion fluorescence in aqueous and organic phases. *J. Less Common Met.* **93**, 331–338 (1983).
23. Barbanel, A. Nephelauxetic effect and hypersensitivity in the optical spectra of actinides. *Radiochim. Acta* **78**, 91–95 (1997).
24. Edelstein, N. M., Klenze, R., Fanghänel, T. & Hubert, S. Optical properties of Cm(III) in crystals and solutions and their application to Cm(III) speciation. *Coord. Chem. Rev.* **250**, 948–973 (2006).
25. Moore, K. T. et al. Failure of Russell-Saunders coupling in the 5*f* states of plutonium. *Phys. Rev. Lett.* **90**, 196404 (2003).
26. Lundberg, D. & Persson, I. The size of actinoid(III) ions – structural analysis vs. common misinterpretations. *Coord. Chem. Rev.* **318**, 131–134 (2016).
27. Sturzbecher-Hoehne, M., Yang, P., D'Aleo, A. & Abergel, R. J. Intramolecular sensitization of americium luminescence in solution: shining light on short-lived forbidden 5*f* transitions. *Dalton Trans.* **45**, 9912–9919 (2016).
28. Booth, C. H. & Hu, Y.-J. Confirmation of standard error analysis techniques applied to EXAFS using simulations. *J. Phys. Conf. Ser.* **190**, 012028 (2009).

Methods

General Considerations

Caution: ^{254}Es ($t_{1/2}$ = 275.7 days, 70.9 TBq g^{-1}) and ^{249}Cf ($t_{1/2}$ = 351 years, 150 GBq g^{-1}) are highly radioactive, and decay to α-, β- and γ-emitting isotopes. These isotopes and their decay daughters present substantial health risks, and were manipulated only in facilities specifically designed for the safe handling of long-lived radioactive materials. All measurements were taken in controlled facilities and/or using multiple containment procedures.

Materials

The ligand HOPO was prepared and characterized as described previously[29], and a ligand stock solution was prepared by direct dissolution of a weighted portion into dimethyl sulfoxide (DMSO). All other chemicals used were obtained from commercial suppliers and used as received.

Preparation of XAS sample

The XAS sample of ^{254}Es/^{249}Cf was assembled from aliquots of the metal and ligand stock solutions, with a final metal-to-ligand ratio of 1:10 and an ^{254}Es concentration of about 17 μM. The ^{254}Es stock (175 ng) was prepped via direct dissolution into 3 M HNO_3 (10 μl) and the final sample was prepared in the stock container. 25 μl of 1 M TRIS was added to buffer the solution and allow for HOPO binding. HOPO was subsequently added (1 μl, 20 mM) and then the sample was buffered to pH 7–8 with an additional 5 μl of 1 M TRIS, resulting in approximately 40 μl of sample. The ^{254}Es(HOPO) solution was dropcast into a 3D-printed sample holder (Extended Data Fig. 7) in increments of 3 μl, and then loaded into an indium-sealed, triply contained aluminium holder with Kapton windows (developed in-house) within one week of synchrotron measurement.

XAS data collection and data treatment

XAS data were collected at the Es L_3 edge on beamline 11-2 at the Stanford Synchrotron Radiation Lightsource using a Si(220) double-crystal monochromator, fully tuned with vertical and horizontal slit sizes of 0.8 mm and 5.5 mm. For these experiments, higher harmonics from the monochromatic light were removed using a 370-mm Rh-coated harmonic rejection mirror. The Rh coating was 50 nm, with 20 nm seed coating, and the substrate was Zerodur. The harmonic rejection cut-off was set at 23500.0 eV by the mirror angle, thereby controlling which photons experience total external reflection. Samples were held in a LN_2-cooled cryostat at 77 K throughout analysis; all XAS measurements were collected in fluorescence mode using a 100-element Canberra Ge detector and corrected for dead time. The data were energy-calibrated to the main edge from a spectrum of Mo foil, setting the first inflection point of the Mo K edge to 20000.0 eV. The dataset consists of 120 scans; sets of 10 scans were averaged into a new file, yielding 12 averaged scans. Owing to high levels of noise, each averaged scan was background-subtracted independently. Data reduction and analysis were conducted using the RSXAP software suite[28,30,31] in conjunction with backscattering line shapes and phases calculated using FEFF9.6[32], which included the EXCHANGE card to apply a +15 eV correction to the Fermi level of the standards. Data were transformed between 2.5 Å^{-1} and 6.6 Å^{-1} using a Gaussian window with a width of 0.3 Å^{-1}. All fitting was conducted in *r* space. Error analysis was performed using a profiling method[28]. In all cases, the total number of fitting parameters was less than two-thirds the total number of independent points.

Owing to limited mass of ^{254}Es in the sample, an extended data acquisition time was required (about 84 h). Over this length of time, beam-induced changes to the sample could occur, and so extended checks on the integrity of the sample were conducted. Extended Data Fig. 4 shows the first eight single XANES spectra collected from the sample with no substantial changes in edge position or structure. Owing to the large amount of data collected on ^{254}Es(HOPO), every 10 scans were merged to give 12 averaged scans. Extended Data Fig. 5 shows these averaged scans from oldest (top) to newest (bottom), demonstrating no apparent changes to the XANES spectra over the length of the measurement. This conclusion was confirmed with measurements of E_0 (as defined by the position of the first inflection point of the main edge) and the main peak or 'white line' position, neither of which showed any change as a function of time throughout the experiment (Extended Data Table 1). Collectively, the data shown in Extended Data Figs. 4 and 5 and in Extended Data Table 1 strongly support the stability of the $[^{254}Es^{III}(HOPO)]^-$ complex throughout the XAS measurement.

The fitting model used for these data is similar to that used previously[2]. Here, the *k* range is more limited, so scattering pairs beyond the Es–C or Es–N shell are not included and water coordination is not considered. Backscattering line shapes and phases were calculated with FEFF9.6[33] using the calculated $[Am^{III}(HOPO)]^-$ structure from ref. [2]. Owing to differences in fit range and the more updated use of the EXCHANGE card mentioned above when calculating the line shapes, there could be some enhanced systematic differences in the An–O bond length results between this and previous studies, and there are probably even larger differences in the Debye–Waller factors.

Because fitting to EXAFS data over such a limited *k* range is not usually reported, we conducted a brief study focusing on the effect of the short *k* range on $[An^{III}(HOPO)]^-$ fits using the data from ref. [2]. For a direct comparison, the older data are refitted using the same model applied to the Es data, so some small differences in the fit results with the original report are expected. Here, we focus on only the average An–O bond length as a function of k_{max}, used in the fit. The results are shown in Extended Data Fig. 3. Although the Cm–O distance remains fairly constant as a function of k_{max}, even for k_{max} as low as 5 Å^{-1}, there are more substantial differences at low k_{max} for Am–O and Cf–O pairs. Using this limited dataset, the maximum bond-length deviation from using a k_{max} of 6.6 Å^{-1} (the value used in the Es data) to a higher k_{max} where the bond length has stabilized is about 0.03 Å.

In the course of this analysis (Extended Data Figs. 8–10), it became clear that there is a glitch in the previously reported Cf data between about 5 Å^{-1} and 5.5 Å^{-1}. Hence, the data at those values of k_{max} are unreliable[2]. This glitch could have had an effect on the previously reported Cf–O bond length, so we have estimated a larger error for that pair in Fig. 2d.

Luminescence spectroscopy

The luminescence sample of ^{254}Es/^{249}Cf was assembled from reprocessing the XAS sample described above. After reprocessing, γ spectroscopy was used to determine ^{254}Es/^{249}Cf activity, which can be used to calculate sample mass, and the γ spectrum was collected on an Ortec IDM-200-V high-purity Ge detector (P-type single crystal; 88 mm diameter, 30 mm length) and calibrated using ^{133}Ba and ^{60}Co point sources. Using the Experimental Unevaluated Nuclear Data List (XUNDL), and owing to discrepancies in the Evaluated Nuclear Structure Data File (ENSDF), the ^{254}Es 2.17% intensity line at 61.89 keV was used to determine the total activity and mass of the sample, which was found to be 38.24 ng of ^{254}Es (ref. [34]). Preparation of the luminescence sample followed a similar protocol to that used for XAS preparation, with ^{254}Es dissolved in 3 M HNO_3 (15 μl) and then partially buffered with 1 M TRIS (25 μl). HOPO was subsequently added (1.5 μl, 20 mM) and then the sample was buffered to pH 7–8 with an additional 40 μl of 1 M TRIS, resulting in approximately 82 μl of sample and a final ^{254}Es concentration of 1.88 μM. Emission and excitation spectra were measured on a Horiba Jobin Yvon Fluorolog-3 spectrofluorometer equipped with a Xe lamp and a near-infrared detector at the Molecular Foundry, using a 10-nm excitation slit and 10-nm emission slit for the excitation spectrum (Extended Data Fig. 6), and a 14-nm excitation slit and a 20-nm emission slit for the emission spectrum, which probably broadened the excitation and emission peaks. In addition, a 0.75-s acquisition time and a Y48 (λ = 480 ± 5 nm) bandpass filter to remove the third harmonic peak were used to collect excitation

and emission spectra. The final spectra were an average of 10 individual measurements.

Data availability

All data are available in the paper. Additional details are available on request to the corresponding authors.

29. Abergel, R. J. et al. Biomimetic actinide chelators: an update on the preclinical development of the orally active hydroxypyridonate decorporation agents 3,4,3-LI(1,2-HOPO) and 5-LIO(Me-3,2-HOPO). *Health Phys.* **99**, 401–407 (2010).
30. Booth, C. H. RSXAP Analysis Package (Berkeley, CA, 2016).
31. Li, G. G., Bridges, F. & Booth, C. H. X-ray-absorption fine-structure standards: a comparison of experiment and theory. *Phys. Rev. B* **52**, 6332–6348 (1995).
32. Ankudinov, A. L., Ravel, B., Rehr, J. J. & Conradson, S. D. Real-space multiple-scattering calculation and interpretation of X-ray-absorption near-edge structure. *Phys. Rev. B* **58**, 7565–7576 (1998).
33. Rehr, J. J., Kas, J. J., Vila, F. D., Prange, M. P. & Jorissen, K. Parameter-free calculations of X-ray spectra with FEFF9. *Phys. Chem. Chem. Phys.* **12**, 5503–5513 (2010).
34. Ahmad, I., Kondev, F. G., Koenig, Z. M., McHarris, W. C. & Yates, S. W. Two-quasiparticle states in ^{250}Bk studied by decay scheme and transfer reaction spectroscopy. *Phys. Rev. C* **77**, 054302 (2008).

Acknowledgements ^{254}Es was supplied by the Isotope Program within the US Department of Energy (DOE), Office of Science, Office of Nuclear Physics. We thank N. Edelstein for discussions, M. Fox for γ spectrometer calibration, and N. Singh, B. Fairchild, S. Hays and R. Davis for assistance in planning and implementing experiments at the Stanford Synchrotron Radiation Lightsource (SSRL) and at the Molecular Foundry. This work was supported by the DOE, Office of Science, Office of Basic Energy Sciences, Chemical Sciences, Geosciences, and Biosciences Division at Lawrence Berkeley National Laboratory, under contract number DE-AC02-05CH1123, and at Los Alamos National Laboratory (LANL), an affirmative-action/equal-opportunity employer, managed by Triad National Security, LLC, for the NNSA of the DOE (contract number 89233218CNA000001). K.M.S. acknowledges support from a DOE Integrated University Program graduate research fellowship. Z.R.J. was supported by the Glenn T. Seaborg Institute at LANL. K.E.K. and J.N.W. were supported by the DOE, Office of Science, Office of Basic Energy Sciences, Early Career Research Program under award DE-SC0019190. J.N.W. was also supported by the DOE, Office of Science, Office of Workforce Development for Teachers and Scientists, Office of Science Graduate Student Research (SCGSR) program, which is administered by the Oak Ridge Institute for Science and Education (ORISE) and managed by ORAU (contract number DE-SC0014664) for the DOE. Use of the SSRL, SLAC National Accelerator Laboratory, is supported by the DOE, Office of Science, Office of Basic Energy Sciences under contract number DE-AC02-76SF00515. Near-infrared luminescence spectra were collected at the Molecular Foundry, a User Facility supported by the DOE, Office of Science, Office of Basic Energy Sciences under contract number DE-AC02-05CH1123.

Author contributions K.P.C., K.M.S., S.A.K. and R.J.A. conceived the study and designed the experiments. K.P.C., K.M.S. and S.A.K. prepared the XAS sample. S.A.K., Z.R.J. and J.N.W. collected XAS data. K.F.S., L.M.M. and C.H.B. analysed XAS results. K.P.C. and K.M.S. prepared the photoluminescence sample. L.A.-S., K.P.C. and T.M.M. collected luminescence data and interpreted the results. All authors discussed the experimental results and contributed to the manuscript.

Competing interests The authors declare no competing interests.

Additional information
Supplementary information The online version contains supplementary material available at https://doi.org/10.1038/s41586-020-03179-3.

Correspondence and requests for materials should be addressed to S.A.K., C.H.B. or R.J.A.

Peer review information *Nature* thanks Louise Natrajan and the other, anonymous, reviewer(s) for their contribution to the peer review of this work. Peer reviewer reports are available.

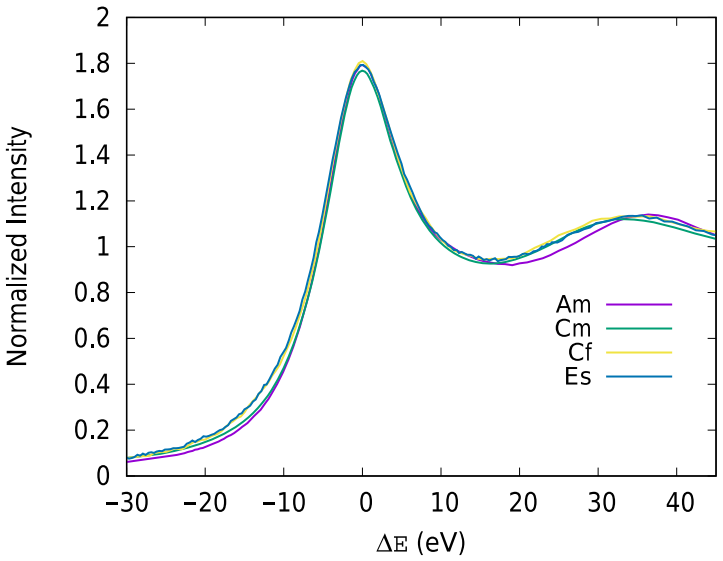

Extended Data Fig. 1 | Comparison of XANES data for $[An^{III}(HOPO)]^-$ complexes. Am^{III}, Cm^{III} and Cf^{III} spectra were reported previously[2] and are compared to the Es^{III} data reported here, when plotted as a function of ΔE, the difference between the photon energy E and the peak in the first derivative of the data E_0.

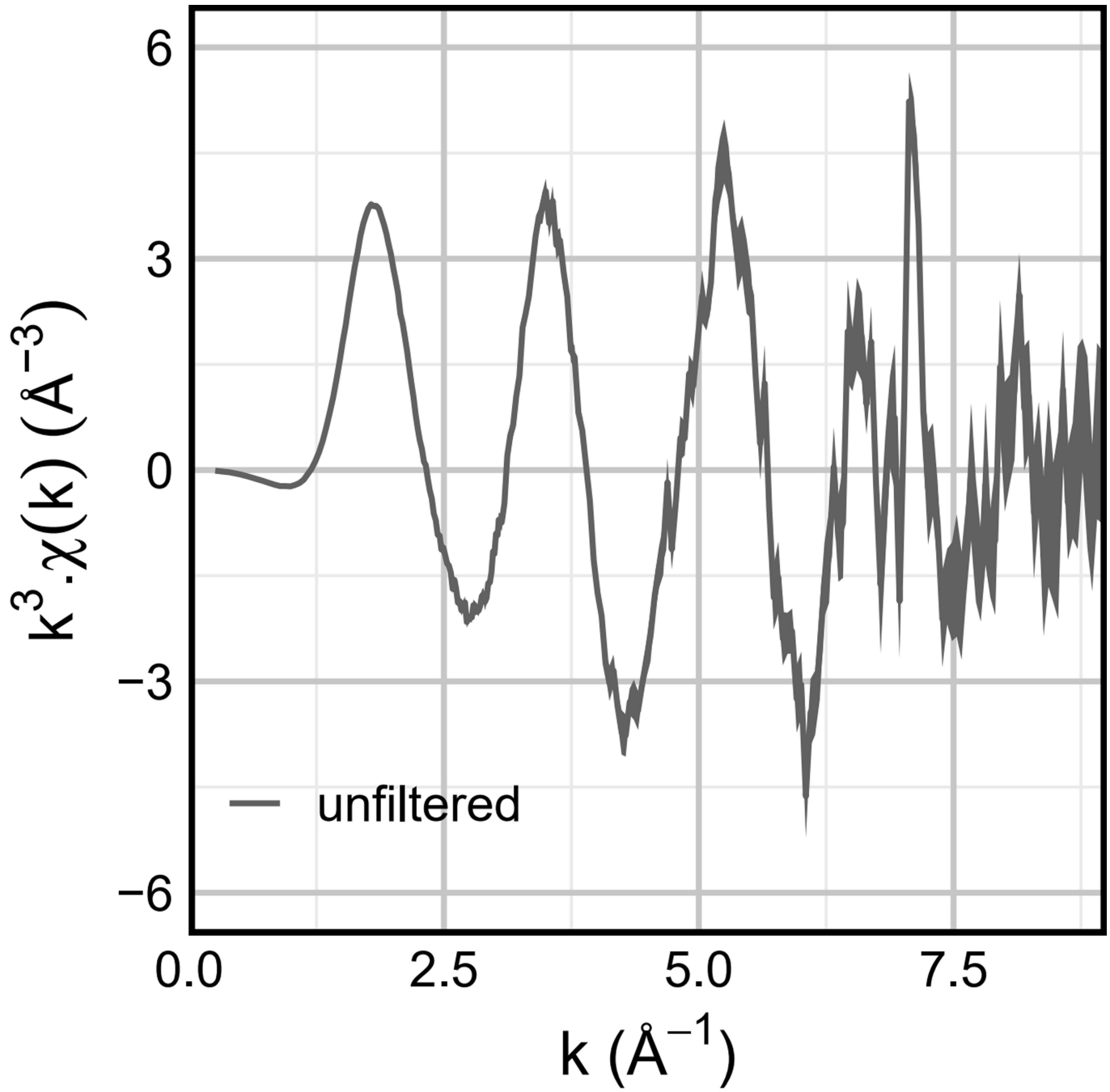

Extended Data Fig. 2 | Raw EXAFS data for $[Es^{III}(HOPO)]^-$. Data are shown as in Fig. 2b, but extended beyond the range used in the fit. The data show the effect of a wide monochromator glitch near 7 Å^{-1} that limited the data range.

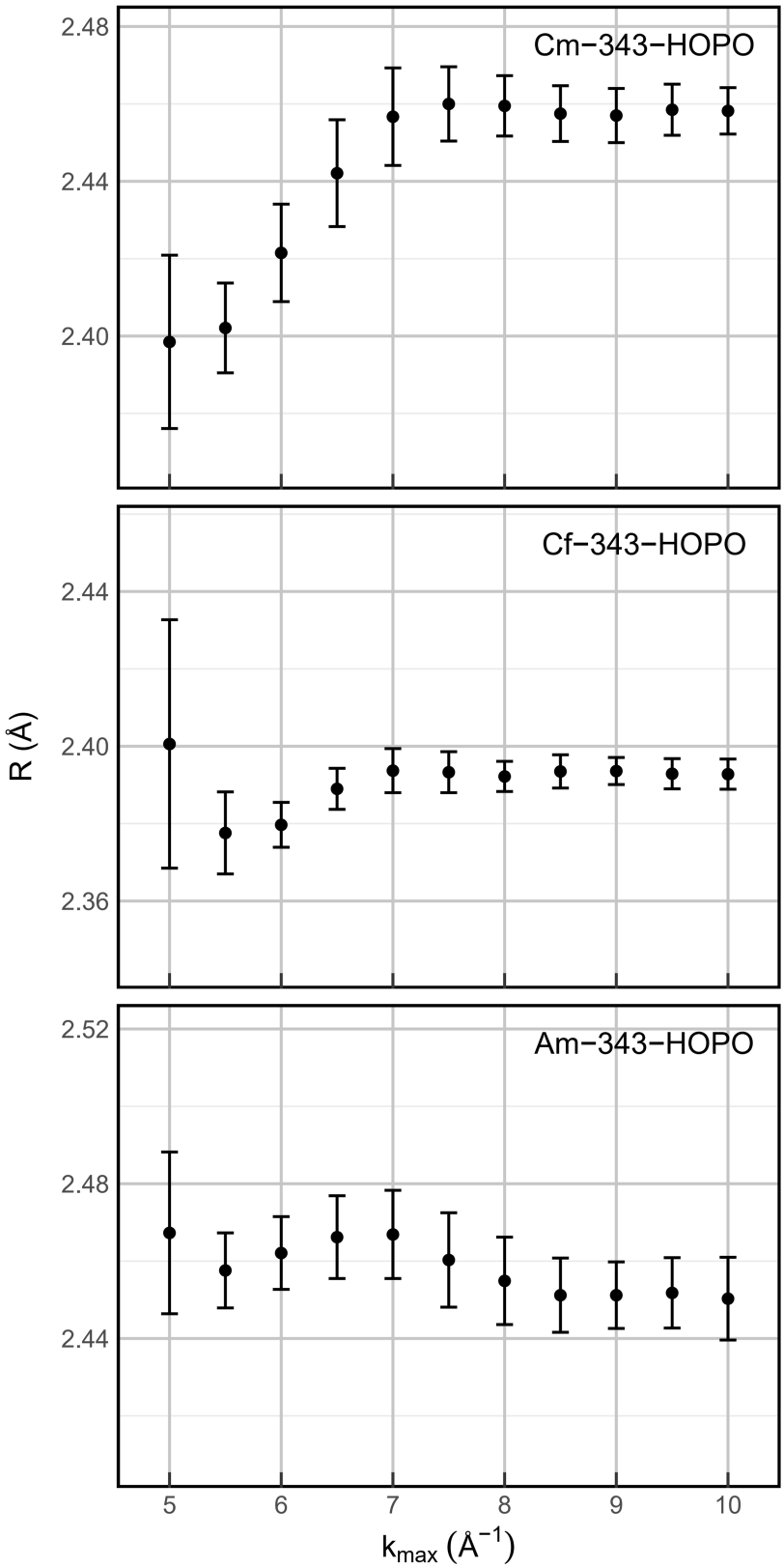

Extended Data Fig. 3 | M–O bond distance *R* versus k_{max} for $[M^{III}(HOPO)]^-$ actinide complexes. These $[M^{III}(HOPO)]^-$ actinide complexes were characterized previously via EXAFS spectroscopy[2]. Note the difference in the fit model from ref. [2] (Methods). The worsening of the fits below 6.5 $Å^{-1}$ is at least partially related to the loss of fit degrees of freedom. For instance, the number of degrees of freedom decreases from 3.3 to 1.2 from k_{max} = 6.5 $Å^{-1}$ to k_{max} = 5.5 $Å^{-1}$. The data for Am^{III} and Cm^{III} are of higher quality because there was more material available. Samples masses are 27.1 µg, 10.9 µg and 3.3 µg for Am^{III}, Cm^{III} and Cf^{III} data, respectively. Reported one-standard-deviation errors are obtained from a previously described profiling method[28].

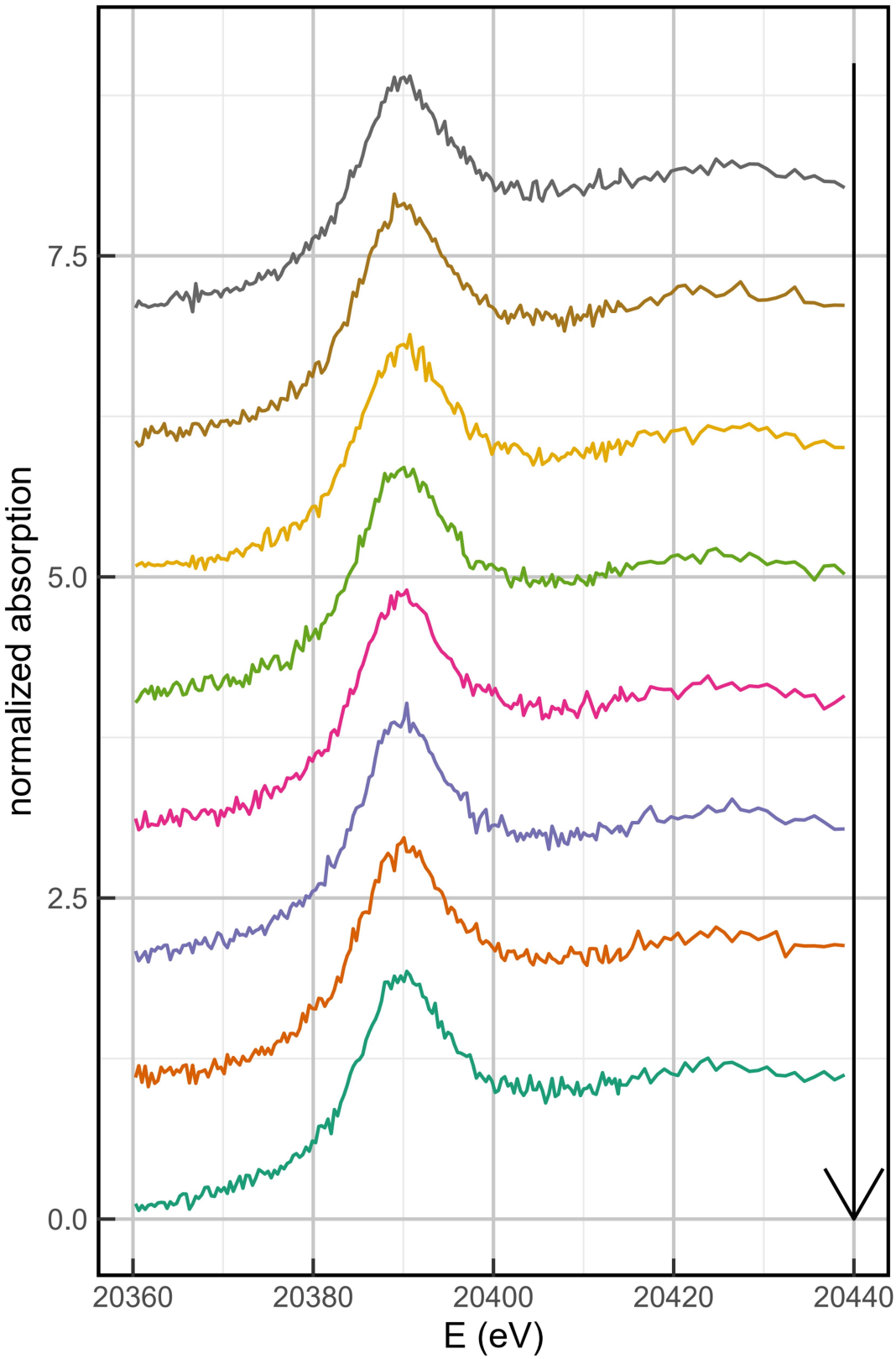

Extended Data Fig. 4 | Comparison of the first eight Es L_3-edge XANES scans collected for $[Es^{III}(HOPO)]^-$ at 77 K. The oldest scan is shown at the top and the newest at the bottom, as indicated by the black arrow. Each scan required about 40 min. Scans are offset for clarity.

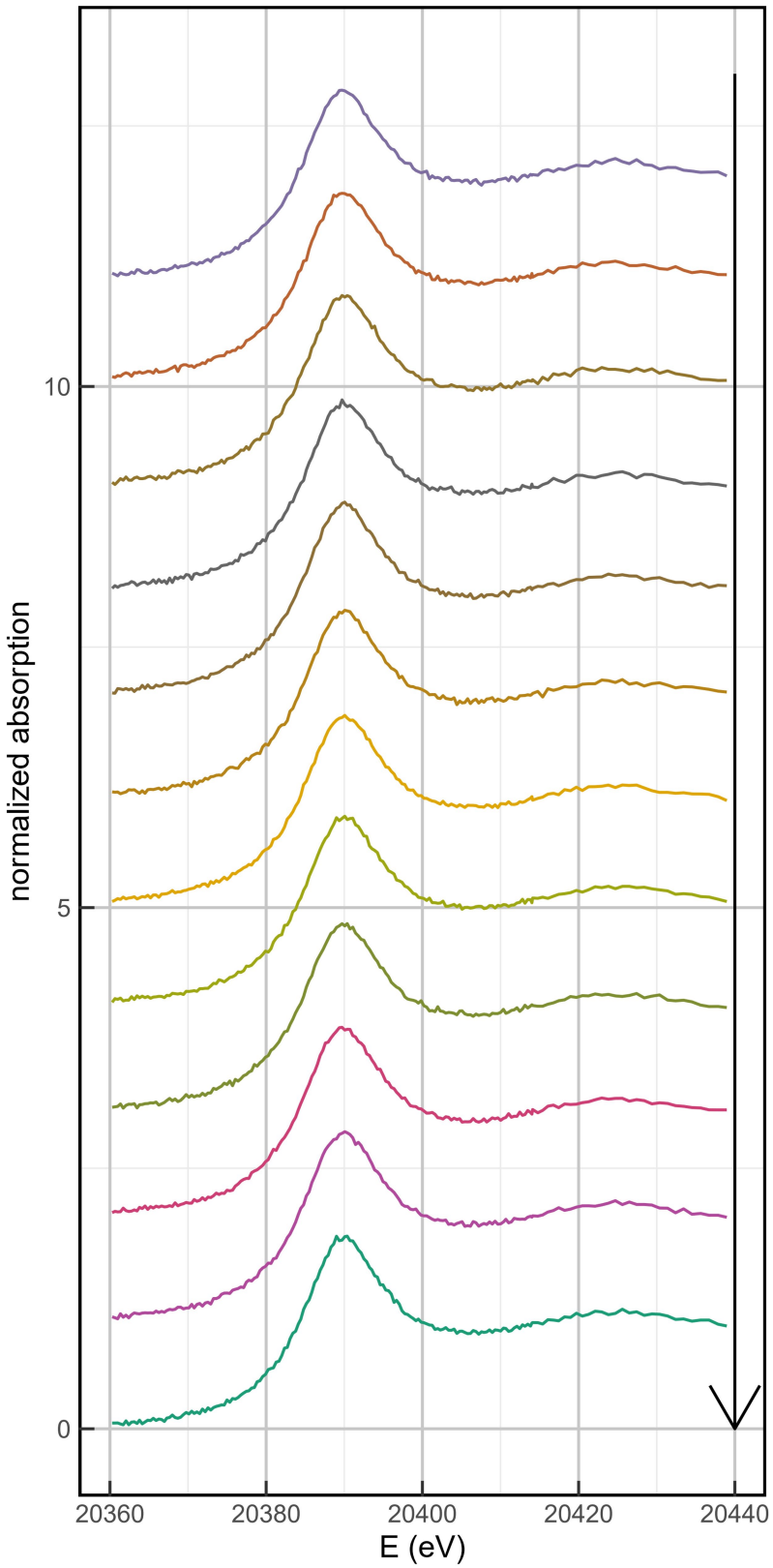

Extended Data Fig. 5 | Comparison of the averaged Es L_3-edge XANES scans collected for $[Es^{III}(HOPO)]^-$ at 77 K. The oldest averaged scan is shown at the top and the newest at the bottom, as indicated by the black arrow. Each averaged scan is taken from 10 individual scans and represents nearly 4 h of data acquisition time. Scans are offset for clarity.

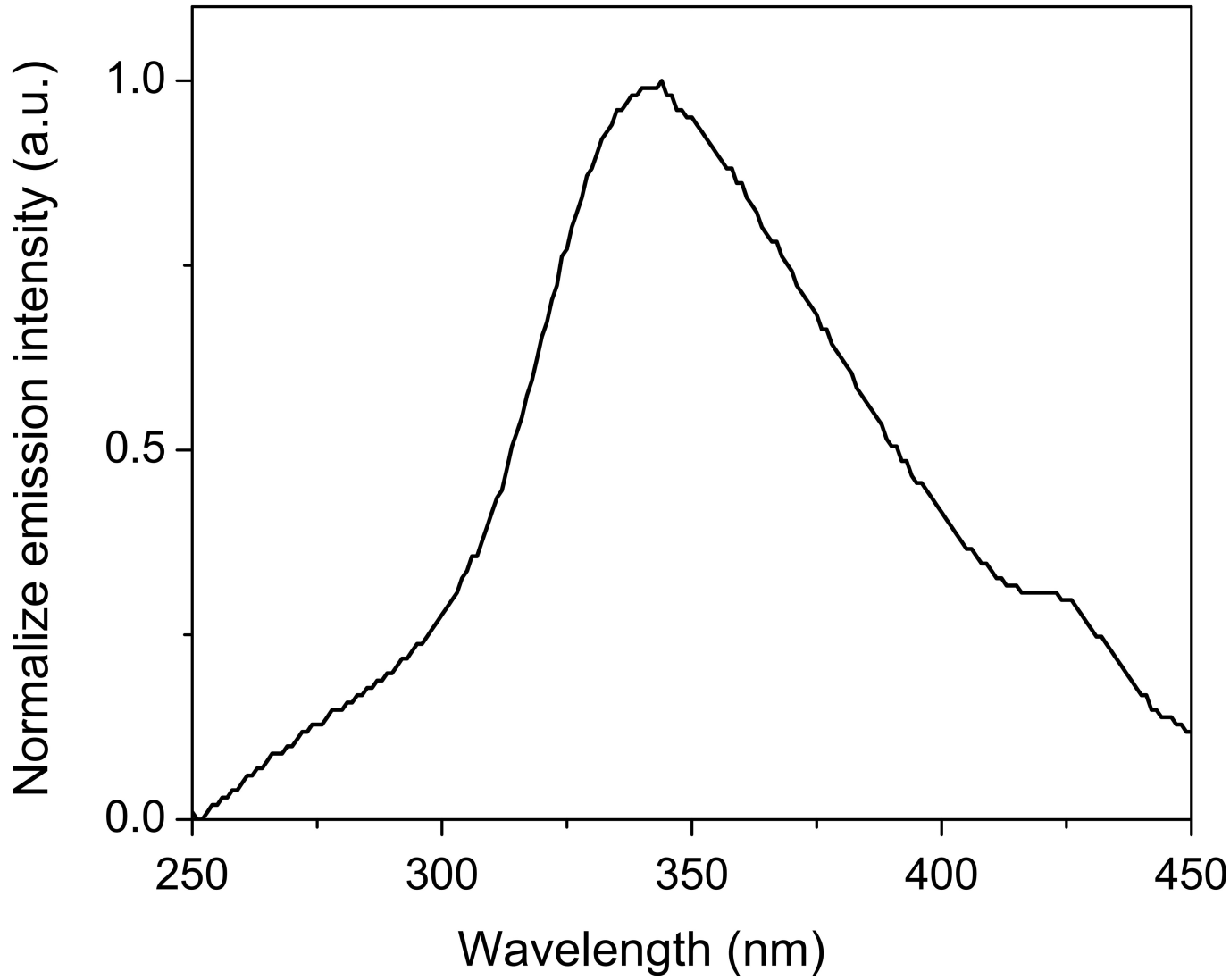

Extended Data Fig. 6 | Normalized excitation spectrum of $[Es^{III}(HOPO)]^-$ in aqueous solution. Spectrum collected on monitoring at Es^{III} emission maximum (1,005 nm).

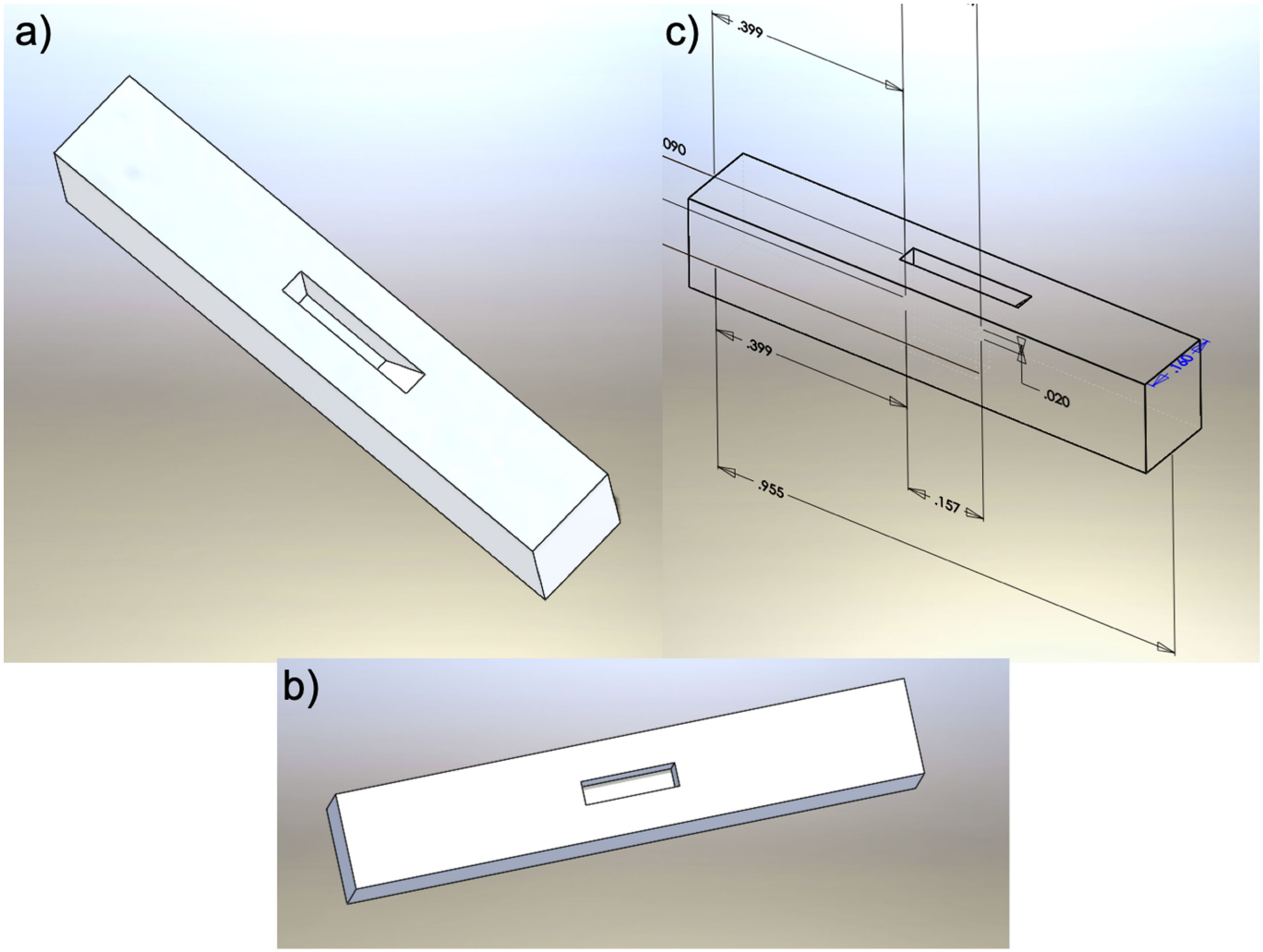

Extended Data Fig. 7 | Schematics of the 3D-printed sample holder used for XAS measurements. a, **b**, Top views of the sample holder. **c**, Computer-aided design (CAD) file for the sample holder.

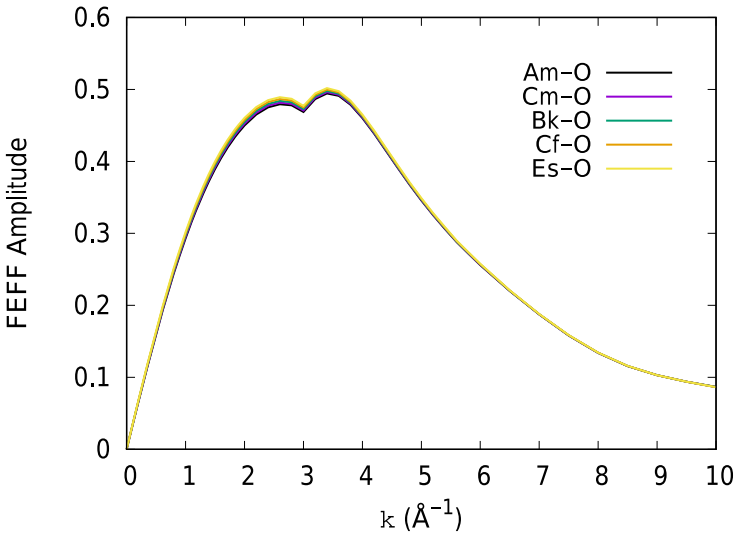

Extended Data Fig. 8 | Comparison of backscattering line shapes and phases for calculated [An^{III}(HOPO)]$^-$ complexes. Backscattering line shapes and phases were calculated using the FEFF code[33] (Methods). The line shapes of the An–O pairs are shown for FEFF calculations using the same structure and varying only the An species to demonstrate the lack of change with species. These amplitudes are not k^3-weighted, as in Fig. 2 and Extended Data Fig. 2, so there is no decrease above 4 Å^{-1} in the line shapes used for fitting, but rather a change in slope.

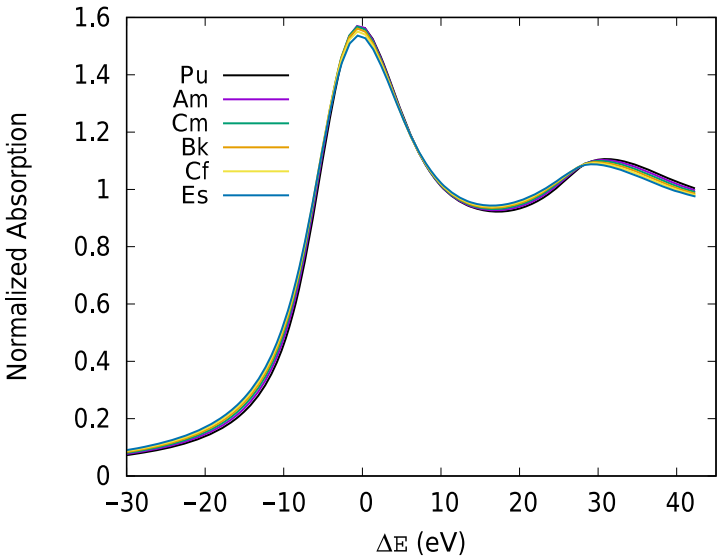

Extended Data Fig. 9 | Comparison of calculated XANES spectra for $[An^{III}(HOPO)]^-$ complexes. Spectra were generated from FEFF9.6 calculations using a self-consistent field cluster of 6 Å and a full-multiple scattering cluster of 4 Å. Calculations on actinides generally overestimate the amount of 5*f* charge transfer when included in the valence orbitals, so these orbitals are treated as core orbitals here. The core–hole lifetime broadening used by the code increases from 8.7 eV to 10.3 eV from Pu^{III} to Es^{III}, the effect of which is visible in the increased broadening of the spectra.

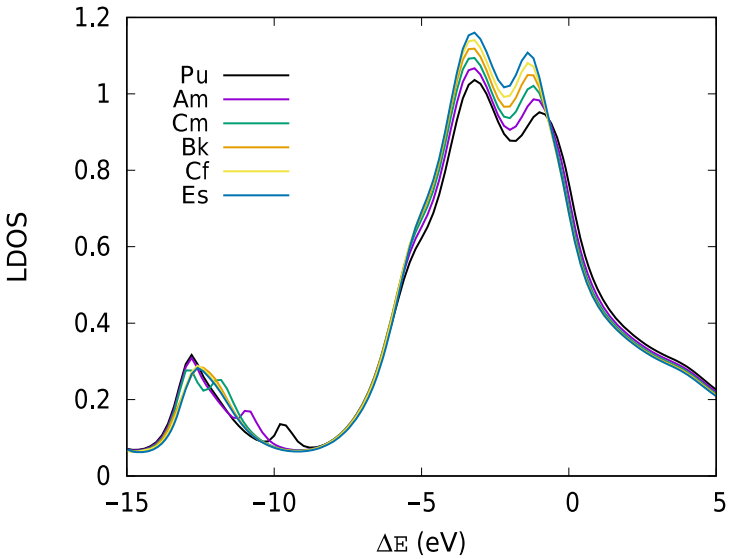

Extended Data Fig. 10 | Comparison of local density of states (LDOS) for the *d* orbitals. The LDOS is determined from the calculations in Extended Data Fig. 9. The spectra are plotted as a function of Δ*E*, the difference between the photon energy *E* and the vacuum energy as calculated by FEFF. The Fermi energy in all these calculations is about −7.6 eV, above which the states are unoccupied and therefore accessible to XANES. The calculations clearly show the 6*d* splitting between −5 eV and 0 eV. The splitting decreases by about 0.6 eV from Pu^{III} to Es^{III}, in contrast to the increase in core–hole lifetime broadening. These effects are washed out in the final calculation in Extended Data Fig. 9 by the much larger core–hole lifetime broadening.

Extended Data Table 1 | Summary of $[Es^{III}(HOPO)]^-$ XAS features

Scan Group (time)	E_0 (eV)	White Line Intensity	White Line Energy (eV)	First Shell FT amplitude
1	20384.5	1.84	20390.0	1.78
2	20386.9	1.85	20390.1	1.81
3	20386.8	1.85	20389.8	1.84
4	20385.0	1.84	20390.0	1.82
5	20385.4	1.87	20390.0	1.82
6	20384.5	1.83	20390.0	1.79
7	20385.5	1.85	20390.1	1.84
8	20385.7	1.88	20390.1	1.75
9	20385.2	1.83	20390.0	1.77
10	20384.0	1.87	20389.9	1.83
11	20385.7	1.85	20389.7	1.80
12	20385.2	1.84	20389.9	1.76
Mean	**20385.4(2)**	**1.85(1)**	**20390.0(1)**	**1.80(1)**
St. Dev.	**0.9**	**0.02**	**0.1**	**0.03**

All energy values are calibrated against the first inflection point of the Mo K-edge set at 20000.0 eV. E_0 is defined as the peak in the first derivative of the Es L_3-edge data from the $[Es^{III}(HOPO)]^-$ sample. FT, Fourier transform; St. Dev., standard deviation of the distribution from the 12 scans. Errors on the mean values (shown in parentheses) represent the standard deviations of the mean for this distribution.

Extended Data Table 2 | Summary of EXAFS fits for $[Es^{III}(HOPO)]^-$

Fit	Shell	N	R (Å)	σ^2 (Å^2)	ΔE_0 (eV)	R (%)
	Es-O	8*	2.38(3)	0.009(2)	0.2(13)	7.5
	Es-C/N	8(4/4)*	3.40(3)	0.012(7)		

N, coordination number assuming an amplitude reduction factor of 1.0; *R* (Å), interatomic distance; σ^2, Debye–Waller factor; ΔE_0, energy shift from the calculated energy of the Fermi level, which had a correction applied in the FEFF calculation (Methods); *R* (%), normalized fit residual[30,31]. The data were transformed over a *k* range of 2.50–6.60 Å^{-1} with a Gaussian window of 0.30 Å^{-1}. The data were fitted over an *R* range of 1.2–3.6 Å, giving 8.3 independent data points. The fit uses five parameters and thus has 3.3 degrees of freedom. Reported errors are based on a profiling method[28] from the fit together with an estimate of probable systematic error from the limited *k* range (Extended Data Fig. 3). *Fixed parameters.

Author Queries

Journal: **Nature**
Paper: **s41586-020-03179-3**
Title: **Structural and spectroscopic characterization of an einsteinium complex**

AUTHOR:
The following queries have arisen during the editing of your manuscript. Please answer by making the requisite corrections directly in the e.proofing tool rather than marking them up on the PDF. This will ensure that your corrections are incorporated accurately and that your paper is published as quickly as possible.

Query Reference	Reference
Q1	Please mention the 'spectroscopic' characterization in the abstract, to tie in with the title
Q2	This proof has been produced on the basis of your corrections to the preproof. For later stage of production we use an online 'eproof' tool, in which you can make corrections directly to the text and mark up corrections to the copyedited figures. Please check that the display items are as follows (ms no: 2020-07-12390): Figs 1–3 (colour); Extended Data display items, 10 figures, 2 tables; SI, no. The eproof will contain the main-text figures edited by us and the Extended Data items (unedited except for the legends). Please check the edits to all main-text figures very carefully, and ensure that any error bars in the figures are defined in the figure legends. Extended Data items may be revised only if there are errors in the original submissions. Please note that the eproof should be amended in only one browser window at any one time, otherwise changes will be overwritten.
Q3	Please check your article carefully, coordinate with any co-authors and enter all final edits clearly in the eproof, remembering to save frequently. Once corrections are submitted, we cannot routinely make further changes to the article.
Q4	Note that the eproof should be amended in only one browser window at any one time; otherwise changes will be overwritten.
Q5	Author surnames have been highlighted. Please check these carefully and adjust if the first name or surname is marked up incorrectly. Note that changes here will affect indexing of your article in public repositories such as PubMed. Also, carefully check the spelling and numbering of all author names and affiliations, and the corresponding email address(es).
Q6	You cannot alter accepted Supplementary Information files except for critical changes to scientific content. If you do resupply any files, please also provide a brief (but complete) list of changes. If these are not considered scientific changes, any altered Supplementary files will not be used, only the originally accepted version will be published.
Q7	If applicable, please ensure that any accession codes and datasets whose DOIs or other identifiers are mentioned in the paper are scheduled for public release as soon as possible, we recommend within a few days of submitting your proof, and update the database record with publication details from this article once available.